PHYSICAL REVIEW B **81**, 085309 (2010)

Transport properties of the two-dimensional interacting anisotropic electron gas at zero temperature

V. S. Khrapai* and A. Gold
Centre d'Elaboration de Materiaux et d'Etudes Structurales (CEMES), CNRS, 29 Rue Jeanne Marvig, 31055 Toulouse, France
(Received 2 September 2009; published 5 February 2010)

At zero temperature we calculate the transport properties of the two-dimensional interacting electron gas in (110) AlAs quantum wells and (110) Si metal-oxide-semiconductor field-effect transistor structures. In these structures the effective mass is anisotropic, which gives rise to anisotropic transport properties. We use the theoretical approach developed by Tokura [Phys. Rev. B **58**, 7151 (1998)], where the conductivity tensor is calculated using the Boltzmann equation. The density dependence of the anisotropic mobility for impurity scattering and for interface-roughness scattering is studied. The predictive power of the theory is demonstrated and we compare with experimental results. For (110) AlAs quantum wells with a mass ratio $m_x/m_y=5.5$ we find mobility anisotropies in the range $1.5<\mu_y/\mu_x<12$.

DOI: 10.1103/PhysRevB.81.085309 PACS number(s): 73.50.−h, 73.61.Ey, 73.21.Fg

I. INTRODUCTION

An anisotropic Fermi surface and/or an anisotropic disorder lead to anisotropic transport properties in semiconductors. This is well known for three-dimensional semiconductors.[1] It is also known that the scattering problem for an anisotropic effective mass and an isotropic scattering potential can be reduced to that of an isotropic effective mass and an anisotropic scattering potential.[1]

In the present paper we consider the anisotropy of transport in the two-dimensional interacting electron gas resulting from an effective-mass anisotropy. We only consider isotropic disorder. Anisotropic transport in the two-dimensional electron gases, as realized in (110) silicon metal-oxide-semiconductor field-effect transistor (MOSFET) structures, was reported long ago.[2] Recently, anisotropic transport was found in (110) AlAs quantum well (QW).[3] Surprisingly, there are only few experimental data on this topic. There exists an early theoretical work for the anisotropic two-dimensional electron gas as realized in silicon (110) MOSFET structures,[4] however, experimental results[2] have not been compared with theory. More recently, Tokura[5] considered anisotropic scattering potentials in the isotropic two-dimensional electron gas using the Boltzmann equation approach. There, the theoretical framework has been given but explicit results for the anisotropic mobility due to an anisotropic Fermi surface have not been presented.

In a recent letter[6] we applied this theory to (110) AlAs QWs and compared our numerical results for the anisotropic transport with the experiment.[3] Excellent agreement was found by assuming that impurities are located at an interface between the QW and an insulating barrier. From this we concluded that the mobility anisotropy in the two-dimensional electron gas could be used to get microscopic insight about disorder. We stress, however, that agreement between theory and experiment only could be obtained[6] within a realistic model, where all extension effects due to the width of the QW have been taken into account.

Transport properties of the two-dimensional electron gas in (100) Si MOSFET (Ref. 7) structures and in (100) AlAs QWs (Refs. 8 and 9) have been studied extensively in experiment. In the (100) plane the effective-mass tensor and the mobility are isotropic. The relevant scattering mechanisms are impurity scattering (IS), which is important at lower carrier density and interface-roughness scattering (IRS), more important at higher electron density. For theoretical work concerning these structures, see Ref. 7 for Si MOSFET structures and Ref. 10 for AlAs QWs. From the results obtained for these isotropic systems it is reasonable to consider these two scattering mechanisms also as the relevant ones in anisotropic systems. In this paper we present our numerical results for IS and IRS for anisotropic (110) AlAs QWs and anisotropic (110) Si MOSFET structures. The effective-mass anisotropy (the ratio of the effective masses along the main symmetry axes) in (110) AlAs QWs (Ref. 3) is 5.5 while in (110) Si MOSFET (Ref. 7) one finds 2.9. According to our calculations, the anisotropy of the transport relaxation time in these two systems can be comparable to that of the effective mass, demonstrating the importance of anisotropic scattering effects.

The paper is organized as follows. In Sec. II we describe the model and the theory. Results concerning the accuracy of our calculations are given in Sec. III. The numerical results for (110) AlAs QWs are presented in Sec. IV. Our results for (110) Si MOSFET structures are given in Sec. V. We discuss our results and the approximations made in Sec. VI. Our conclusions are given in Sec. VII.

II. MODEL AND THEORY

A. Model

In the following we consider an interacting two-dimensional electron gas in the xy plane and we suppose that the in-plane effective-mass tensor is diagonal with two effective masses m_x and $m_y<m_x$. The value of the effective mass m_z perpendicular to this plane is important for the IRS in the case of QWs and for confinement effects in the case of MOSFET structures. When considering a QW we suppose infinite barriers at $z=0$ and $z=w$ and the electron gas is located at $0<z<w$ with a wave function in z direction given by $\xi_0(0<z<w)\propto\sin(\pi z/w)$. The width parameter in such a

 ©2010 The American Physical Society

system is the QW width w and explicit results for the mobility depend on its value. For Si MOSFET structures we use the triangular confinement potential where the effective penetration of the Fang-Howard wave function $\xi_0(z<0)\propto z\exp(bz/2)$ into the semiconductor is given by $z_0=-3/b$ and b is the Stern and Howard confinement parameter.[7] b is determined by $b=[48\pi m_z e^2 N^*/\varepsilon_{sc}\hbar^2]^{1/3}$ with $N^*=N_{Depl}+11N_S/32$, where N_S is the electron density and N_{Depl} the depletion charge density.[7] ε_{sc} is the dielectric constant of the semiconductor, Si in our case. In the case of MOSFET structures (or heterostructures) the width of the electron gas is determined by b and is not an independent parameter as in the case of QWs.

We consider two scattering processes caused by disorder: IS and IRS. Suppose that there is a disorder due to randomly distributed charged impurities of density N_I in the xy plane at a distance z_I from the origin. For QWs $z_I=w/2$ corresponds to impurities located at the center of the QW and for $z_I=0$ (or $z_I=w$) the impurities are located at the edge of the QW. In MOSFET structures $z_I=0$ corresponds to impurities located at the interface between the semiconductor (Si, $z<0$) and the oxide (SiO_2, $z>0$); for $z_I>0$ the impurities are located in the oxide. The Fourier transform of the unscreened random potential is written as $\langle|U(\vec{q})|^2\rangle=N_I[2\pi e^2F_I(q,z_I)/\varepsilon_L q]^2$. $F_I(q,z_I)$ represents the impurity form factor, which also depends on w if QWs are considered and it depends on b in the case of MOSFET structures. Explicit expressions can be found in Ref. 7 for MOSFET structures and in Ref. 11 for QWs. We mention that in the long-wavelength limit one gets $F_I(q=0,z_I)=1$. ε_L is the dielectric constant of the background material.

We also consider IRS, which is described by Δ, the average height of the interface roughness in the z direction and by Λ, the correlation length parameter of the interface roughness in the xy plane. For QWs (Ref. 12) we use $\langle|U(\vec{q})|^2\rangle=2\pi^5\Delta^2\Lambda^2\exp(-q^2\Lambda^2/4)/(w^6m_z^2)$. In thin QWs this scattering mechanism becomes dominant and the mobility μ increases according to $\mu\propto w^6$. Note that a smaller value of m_z increases the IRS. For Si MOSFET structures we use the expression[7,13]

$$\langle|U(\vec{q})|^2\rangle=4\pi^3e^4\Delta^2\Lambda^2(N_S+2N_{Depl})^2\exp(-q^2\Lambda^2/4)/\varepsilon_L^2.$$

Because of $\langle|U(\vec{q})|^2\rangle\propto N_S^2$ IRS becomes dominant at high electron density: with increasing N_S the electron gas is pushed toward the interface and IRS increases.

Coulomb interaction effects are treated within the random-phase approximation which leads to conventional screening of the random potential by a q-dependent dielectric function $\varepsilon(\vec{q})=1+q_SF_C(q)/q$.[7] $q_S=2g_v/a_B^*$ is the screening wave number given by the valley degeneracy g_v and the effective Bohr radius $a_B^*=a_B\varepsilon_L m_e/m_D$, defined by the density-of-states mass $m_D=\sqrt{m_xm_y}$ and the Bohr radius of the hydrogen atom $a_B=0.529$ Å. $F_C(q)$ represents the form factor for the Fourier-transformed Coulomb interaction potential $V(\vec{q})=2\pi e^2F_C(q)/\varepsilon_L q$ in the two-dimensional electron gas. Explicit expressions of $F_C(q)$ for MOSFET structures can be found in Ref. 7 and for QWs in Ref. 11. $F_C(q)$ depends for QWs on w and for MOSFET structures on b. In the long-wavelength limit, again, one finds $F_C(q\rightarrow 0)=1$.

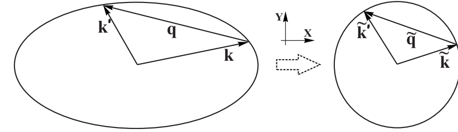

FIG. 1. Illustration of the Herring-Vogt-type transformation of an elliptic Fermi surface ($\vec{k}$) to a spherical Fermi surface ($\vec{\tilde{k}}$).

B. Theoretical framework

The theoretical approach developed in Ref. 5 is a transport theory for electrons in two dimensions with an isotropic mass in the presence of anisotropic scattering potentials. In the present paper we consider a screened random potential which is isotropic, however, the kinetic energy of the electrons is anisotropic, owing to the anisotropic mass. With a Herring-Vogt-type[1] transformation one can transform the anisotropic kinetic energy $E(\vec{k})=\frac{\hbar^2k_x^2}{2m_x}+\frac{\hbar^2k_y^2}{2m_y}$ of a particle into an isotropic form $E(\vec{\tilde{k}})=E_F[(k_x/k_x^F)^2+(k_y/k_y^F)^2]=E_F\tilde{k}^2$, where we introduced[14] the dimensionless vector $\tilde{k}_i\equiv k_i/k_i^F$ for $i=x,y$ with k_i^F defined by $E_F=\frac{\hbar^2k_x^{F^2}}{2m_x}=\frac{\hbar^2k_y^{F^2}}{2m_y}$, see Fig. 1.

Initially, the screened random potential in Fourier space is isotropic and depends only on $q=|\vec{q}|=|\vec{k}-\vec{k}'|$. With the Herring-Vogt-type transformation this variable is transformed to $\tilde{q}=|\vec{\tilde{q}}|=|\vec{\tilde{k}}-\vec{\tilde{k}}'|$. The wave number q is given in terms of $\tilde{q}$ by $q=\tilde{q}q_F\sqrt{1+\alpha\cos(2\psi)}$. ψ is the angle between $\vec{\tilde{q}}$ and the x axis, see Fig. 1. The parameter α describes the anisotropy of the mass tensor and is given by $\alpha\equiv\frac{m_x-m_y}{m_x+m_y}$ and $q_F\equiv\sqrt{\pi N_S(m_x+m_y)/(g_vm_D)}$ is a wave number. We note that for $m_x=m_y$ the anisotropy parameter vanishes, $\alpha=0$, and the transformed screened random potential is isotropic $q=\tilde{q}q_F$ with $q_F=k_F$ and $k_F=(2\pi N_S/g_v)^{1/2}$ is Fermi wave number of the isotropic electron gas. For $m_x\neq m_y$ the screened random potential becomes anisotropic in the transformed coordinates due to the ψ dependence of q. We conclude that after the Herring-Vogt-type transformation we are left with a Hamiltonian with an isotropic kinetic energy and with an anisotropic screened random potential. After this transformation we can apply the theoretical framework of Ref. 5 to calculate the two (elastic) scattering times τ_x and τ_y of the anisotropic transport.

The theoretical approach,[5] which we use for our calculations, is described as follows. A relaxation-time vector is used to express the nonequilibrium part of the distribution function, which enters the Boltzmann equation.[15] The input function in this approach is the screened random potential as the scattering function $Q(q)=Q(\tilde{q},\psi)\propto\langle|U(\tilde{q},\psi)|^2\rangle/\varepsilon(\tilde{q},\psi)^2$. The unscreened scattering function is calculated in Born approximation, which corresponds to the random potential introduced earlier, however, expressed with the new variables to assure an isotropic kinetic energy.

It was shown that the corresponding conductivity tensor is diagonal ($\sigma_{xy}=\sigma_{yx}=0$) by assuming two symmetry axes of the scattering function. Then $Q(\tilde{q},\psi)$ is developed in a Fourier series given by $Q(\tilde{q},\psi)=\sum_{m=0}^{\infty}Q_m(\tilde{q})\cos(2m\psi)$ with the inversion expressed as $Q_m(\tilde{q})=\frac{1}{\pi(1+\delta_{m,0})}\int_0^{2\pi}d\psi Q(\tilde{q},\psi)\times\cos(2m\psi)$. Here we use $\delta_{nm}=0$ for $n\neq m$ and $\delta_{nm}=1$ for $n=m$.

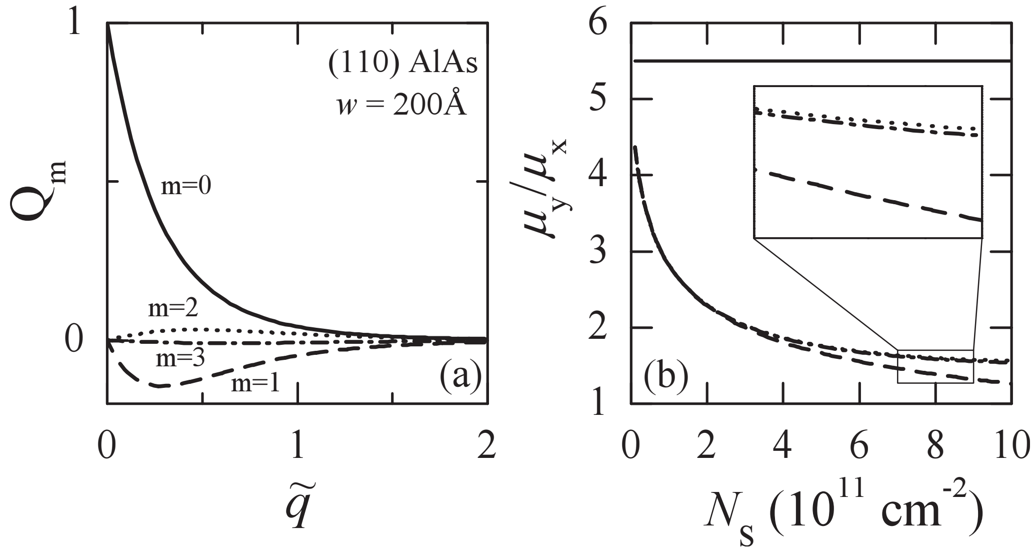

FIG. 2. Impurity scattering in an (110) AlAs quantum well of width w=200 Å with $N_I=1\times10^{10}$ cm^{-2} and z_I=0. (a) Scattering probability $Q_m(\tilde{q})$ for m=0,1,2,3 versus dimensionless wave number $\tilde{q}$ for $N_S=1\times10^{12}$ cm^{-2}. (b) Mobility ratio μ_y/μ_x versus electron density N_S. For the solid line $Q_0(\tilde{q})$ is taken into account. For the dashed line $Q_0(\tilde{q})$ and $Q_1(\tilde{q})$ are taken into account. For the dotted line $Q_0(\tilde{q})$, $Q_1(\tilde{q})$, and $Q_2(\tilde{q})$ are taken into account and for the dashed-dotted line all $Q_m(\tilde{q})$ with m=0–3 are taken into account.

The two integral equations for the two scattering times obtained from the Boltzmann equation are solved by Fourier expansion. The two solutions are written in terms of two infinite symmetric matrices $K^x_{l,n}$ and $K^y_{l,n}$, which are given as functions of the matrix $J_{n,m}=\int_0^{2\pi}d\zeta Q_n(\tilde{q}_\zeta)[\cos(n\zeta)-\cos(m\zeta)]$ with $\tilde{q}_\zeta=2k_F\sin|\zeta/2|$, where ζ is a scattering angle in the transformed momentum space. We note that in order to calculate $J_{n,m}$ two integrations $d\psi d\zeta$ over $Q(\tilde{q}_\zeta,\psi)$ have to be performed. With $K^{x/y}_{l,n}=(-1)^{l-n}[(1+\delta_{l,n})J_{|l-n|,n+l-1}\mp J_{n+l-1,|l-n|}]/2$ (the − sign is for $K^x_{l,n}$ and the + sign for $K^y_{l,n}$) one can calculate the scattering times $\tau_x=(K^x)^{-1}_{1,1}$ and $\tau_y=(K^y)^{-1}_{1,1}$ via a matrix inversion. The corresponding mobilities and conductivities, respectively, are given by the scattering times via $\mu_i=e\tau_i/m_i$ and $\sigma_{ii}=N_Se\mu_i$ for $i=x,y$.

$Q_0(\tilde{q})$ describes isotropic scattering while $Q_1(\tilde{q})$ is the most important term of the anisotropic contributions to the scattering function. For isotropic masses one finds $Q_0(\tilde{q})>0$ while $Q_m(\tilde{q})=0$ for $m=1,2,\ldots$. In this case the two scattering times τ_x and τ_y are identical and are given by the known expression for an isotropic system, which is determined by $Q_0(\tilde{q})$. Details are discussed in Sec. III B.

C. Material parameters

In the following we choose the x and y coordinates axes along the two symmetry axes in the (110) AlAs or (110) Si plane and the z axis along the [110] confinement direction. In these coordinates the in-plane effective-mass tensor of the two-dimensional electron gas becomes diagonal with two effective masses $m_x=m_l$ and $m_y=m_t$ with $m_l>m_t$.

The material parameters used for (110) AlAs are as follows. The effective-mass tensor of the electron gas in the xy plane is given by $m_x=1.1m_e$ and $m_y=0.2m_e$, where m_e is the free-electron mass.[3] The IRS is determined by $m_z=0.2m_e$ and the electron gas has a valley degeneracy $g_v=1$. Due to the small mass m_z IRS is very important in (110) AlAs QWs. The dielectric constant is $\varepsilon_L=10.16$.[16]

For the (110) Si surface we use for the effective masses $m_x=0.553m_e$ and $m_y=0.19m_e$.[7] The confinement parameter b is determined by $m_z=0.315m_e$. In theory the valley degeneracy for the (110) Si surface is $g_v=4$. But $g_v=2$ (Refs. 17 and 18) and $g_v=4$ (Refs. 19 and 20) have been found in experiment. We perform calculations for both values. We use for the depletion charge density $N_{Depl}=1\times10^{11}$ cm^{-2}. For the dielectric constant of the semiconductor (Si) we apply $\varepsilon_{sc}=11.5$ and for the insulator (SiO_2) we use $\varepsilon_{ins}=3.9$. The dielectric constant of the background is given by $\varepsilon_L=(\varepsilon_{sc}+\varepsilon_{ins})/2=7.7$.

III. GENERAL RESULTS

In this section we illustrate the accuracy of our calculations and discuss some general properties of the scattering function $Q(q)$.

A. Numerical

In order to perform numerical calculations the infinite symmetric matrices $K^x_{l,n}$ and $K^y_{l,n}$, which determine the scattering times, must be truncated to a finite size. The infinite expansion of $Q(\tilde{q},\psi)$ must be truncated, too. The numerical results shown in this paper have been calculated with 5×5 matrices for $K^{x/y}_{l,n}$ $(l,n=1,2,\ldots,5)$ with four elements for $Q_m(\tilde{q})$ $(m=0,1,2,3)$.

In Fig. 2(a) we show the Fourier elements $Q_m(\tilde{q})$ $(m=0,1,2,3)$ for IS versus $\tilde{q}$ for an AlAs QW with the largest width used (w=200 Å) and for $N_S=1\times10^{12}$ cm^{-2}. Here, the impurities are located at the edge of the QW. With increasing m the contributions $Q_m(\tilde{q})$ become small compared to $Q_0(\tilde{q})$ and the term $Q_3(\tilde{q})$ is already very small. We have studied the effect of the different contributions $Q_m(\tilde{q})$ to the

mobility anisotropy. This is shown in Fig. 2(b) where we plotted μ_y/μ_x versus electron density N_S for this QW. The solid line is calculated with $Q_0(\tilde{q})$ and the mobility ratio is given by the mass ratio, which means that the scattering time is isotropic. The dashed line in Fig. 2(b) is calculated with $Q_0(\tilde{q})$ and $Q_1(\tilde{q})$. This is the lowest-order approximation giving rise to anisotropy of the scattering time. We find that with increasing N_S the mobility ratio is strongly reduced, i.e., the scattering time is strongly anisotropic ($\tau_y/\tau_x<1$) and this anisotropy increases with increasing density. The dotted line in Fig. 2(b) is calculated using $Q_0(\tilde{q})$, $Q_1(\tilde{q})$, and $Q_2(\tilde{q})$. At low density the dotted and dashed lines are practically coincident, though differences up to 15% between the two lines arise with increasing the density toward $N_S=10^{12}$ cm^{-2}. This means that attaining just two terms in $Q_m(\tilde{q})$ is enough in the density range $N_S<3\times10^{11}$ cm^{-2}. Note that the smaller the QW width the larger is the validity range of this approximation. Finally, for the dashed-dotted line all $Q_m(\tilde{q})$ with $m=0-3$ are used. The differences between the dashed-dotted and dotted lines are negligible in the entire density range [see the enlarged scale in the inset of Fig. 2(b)]. This demonstrates that the numerical calculations are sufficiently accurate for the parameter space used in the present paper.

B. Small anisotropy

Now, we discuss in more detail the approximation $Q(\tilde{q},\psi)=Q_0(\tilde{q})+Q_1(\tilde{q})\cos(2\psi)$. In this case the matrices $K^x_{l,n}$ and $K^y_{l,n}$ contain many zeros and the matrix inversion, in order to determine the scattering time, is simplified. Using for an isotropic factor the approximation $\Gamma_3(1)=0$ one finds for the scattering times the simple expressions $1/\tau_x=J_{0,1}-J_{1,0}/2$ and $1/\tau_y=J_{0,1}+J_{1,0}/2$.[5] Two matrix elements $J_{0,1}=\int_0^{2\pi}d\zeta Q_0(\tilde{q}_\zeta)(1-\cos\zeta)$ and $J_{1,0}=\int_0^{2\pi}d\zeta Q_1(\tilde{q}_\zeta)(1-\cos\zeta)$ determine the anisotropic scattering times. The approximation is valid for small anisotropy of the scattering times because only the lowest anisotropic contribution $Q_1(\tilde{q})$ has been taken into account. According to Fig. 2(b), see the dashed line, the validity range of small anisotropy for impurity scattering is the low N_S range. For $J_{1,0}\ll J_{0,1}$ one finds $\mu_y/\mu_x\cong m_x(1-J_{1,0}/J_{0,1})/m_y<1$, which shows for small anisotropy the deviations from the mass ratio.

For an isotropic mass tensor one finds $Q_1(\tilde{q})=0=J_{1,0}$ and the scattering times are given by $1/\tau_x=1/\tau_y=J_{0,1}=\int_0^{2\pi}d\zeta Q(\tilde{q}_\zeta)(1-\cos\zeta)$, where we used that for an isotropic mass tensor $Q(\tilde{q})=Q_0(\tilde{q})$. This is the well-known formula for isotropic transport.[7]

C. Scattering function $Q(q)$

In the following we discuss the realizations of the scattering function $Q(q)$. First of all we consider an electron gas without screening effects. For a short-range disorder and without screening the random potential does not depend on q and is not modified by a Herring-Voigt-type transformation. Therefore $Q(\tilde{q},\psi)=Q(\tilde{q})=Q_0(\tilde{q})$ does not depend on ψ (i.e., it is isotropic) and consequently one finds $\tau_x=\tau_y$. Correspondingly, the mobility ratio is given by the mass ratio $\mu_y/\mu_x=m_x/m_y$, independent of N_S. We conclude that all deviations of μ_y/μ_x from the mass ratio are due to interaction effects (screening) and/or a long-range random potential. This is an important result.

For IS the scattering function is expressed by $Q(q)\propto N_I F_I(q,z_I)^2/[F(q)+q/q_S]^2$ and for small wave number given by $Q(q\to0)\propto N_I(1+aq)$, where in the general case a is negative (but not always) and depends on the position of impurities, the well width, and q_S. We conclude that for very small wave number the screened random potential for IS behaves like a short-range random potential without screening.

For the isotropic two-dimensional electron gas it is well known that the inverse scattering time $1/\tau$ is determined by a q integral over the screened random potential, where the most important contributions are due to backscattering, which means for $q=2k_F$.[7] This argument also allows to understand quantitatively the situation for the anisotropic case, where $k_x^F>k_y^F\propto m_y^{1/2}$. Since $1/\tau_x\propto Q(2k_F^x)<Q(2k_F^y)\propto1/\tau_y$ for $a<0$ we conclude that $\tau_y/\tau_x<1$ if IS is considered. For very small N_S the corresponding k_x^F and k_y^F are such small that the screened random potential is nearly constant and one approaches $\tau_y/\tau_x\to1$. This limit has been studied before[14] and appears to have a very small validity range, see Fig. 2(b).

The origin of the deviations from $\mu_y/\mu_x=m_x/m_y$ is the q dependence of the screened random potential, generated by screening effects and the two form factors due to the finite width and the position of impurities. For an ideal two-dimensional electron gas of zero width with $F_C(q)=1$ and $F_I(q)=\exp(-|z_I|q)$ on gets $Q(q)\propto N_I\exp(-2|z_I|q)/(1+q/q_S)^2$ and the scattering function decays strongly with increasing q. This q dependence of $Q(q)$ is stronger if width effects are taken into account and even stronger if impurities are located at the edge or outside the QW.[6] For IS the mobility anisotropy decreases with increasing density, see Fig. 2(b). This implies that the scattering times anisotropy increases with increasing density and $\tau_y<\tau_x$. Numerical results of μ_y/μ_x for IS will be discussed later in Secs. IV and V.

For IRS the scattering function is given by $Q(q)\propto q^2\Delta^2\Lambda^2\exp(-q^2\Lambda^2/4)/[F_C(q)+q/q_S]^2$ and for small wave number one gets $Q(q\to0)\propto q^2\Delta^2\Lambda^2$. Because of $1/\tau_x\propto Q(k_F^x)>Q(k_F^y)\propto1/\tau_y$ we conclude that $\tau_y/\tau_x>1$ for IRS. The strong increase in $Q(q)$ with wave number is the reason why we find numerically $\mu_y/\mu_x>m_x/m_y$ with $\tau_y>\tau_x$ for low N_S in the case of IRS. This means that even for low density the scattering times are strongly anisotropic in the case of IRS, quite different from IS. In the case of IRS $Q(q)$ shows a maximum near $q\approx1/2\Lambda$ and for larger q values the scattering function $Q(q)$ decays rapidly. Therefore, one expects that for very large density $N_S\gg N_\Lambda^*=g_v/(32\pi\Lambda^2)$ one again finds $\mu_y/\mu_x<m_x/m_y$.

Numerically, see later, we shall find $\mu_y/\mu_x\approx2m_x/m_y$ for low density $N_S<N_\Lambda^*$, which means $\tau_y\approx2\tau_x$. The unscreened IRS potential is short range for small wave number. We conclude that the anisotropy of the scattering times $\tau_y\approx2\tau_x$ is a consequence of the Coulomb interaction. Numerical results for IRS will be discussed later in Secs. IV and V.

IV. (110) ALUMINUM-ARSENIT QUANTUM WELLS

Calculation of absolute values of the mobility requires a knowledge of the disorder potential. The experimental value

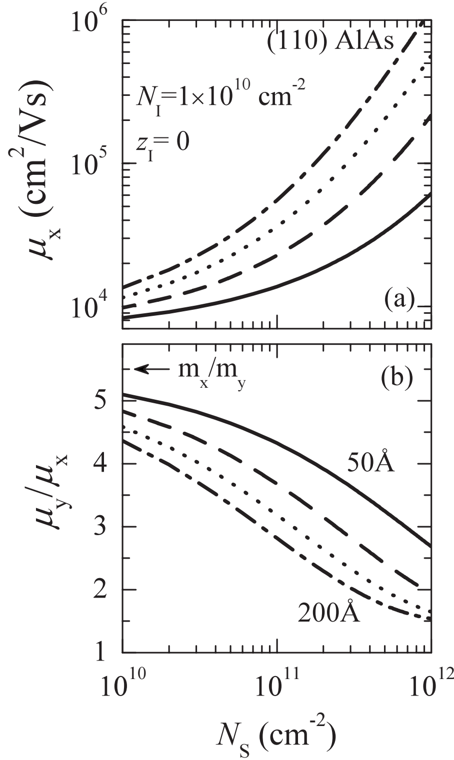

FIG. 3. (a) Mobility μ_x and (b) mobility ratio μ_y/μ_x versus electron density N_S for (110) AlAs QWs for IS with impurities located at the edge of the QW for different well width w=50 Å (solid line), w=100 Å (dashed line), w=150 Å (dotted line), and w=200 Å (dashed-dotted line). The arrow represents the mass ratio.

for the mobility in the (110) AlAs QW was $\mu_x \approx 3 \times 10^4$ cm^2/V s for $N_S \approx 1.65 \times 10^{11}$ cm^{-2} (for w=150 Å with μ_y/μ_x=2.8).[3] At such a low density in a relatively wide quantum well the mobility is likely to be limited by the IS. This allows us to choose the impurity concentration of $N_I \approx 1 \times 10^{10}$ cm^{-2} in our figures for AlAs QWs. For the IRS experimental results are not available in the literature and we use reasonable values of the parameters Δ=3 Å and Λ=30 Å.

We have recently published some numerical results for the mobility ratio μ_y/μ_x of (110) AlAs QWs for impurities located at the center and at the edge of the (110) AlAs QW.[6] There it was shown that perfect agreement with experiment[3] can be found if impurities are located at the edge of the QW. We stress that agreement with experiment was found only by taking into account the Coulomb interaction with all form factors due to the finite width.[6] In the following we present additional results for IS and IRS.

The mobility μ_x and the mobility ratio μ_y/μ_x for IS and impurities at the QW edge versus density N_S are shown in Fig. 3. With increasing N_S the mobility increases, due to screening. The increase in the mobility with w is owing to the increase in the distance between the impurity layer at z_I=0 and the center of the electron gas at $z=w/2$. Note that the value of the mobility is inversely proportional to the impurity density so that Fig. 3(a) can be used to determine N_I from an experimental value μ_x. The ratio μ_y/μ_x decreases with N_S

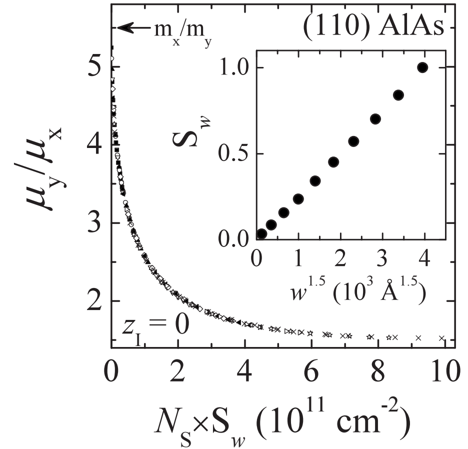

FIG. 4. Mobility ratio μ_y/μ_x versus $N_S \times S_w$, where N_S is the electron density and S_w a dimensionless scaling factor, for (110) AlAs QWs for IS with impurities located at the edge of the QW. Different symbols represent different well width. In the inset we show S_w versus $w^{3/2}$ for QWs of width 40 Å$<w<$250 Å.

and increasing w, due to screening and the form factors F_I and F_C. We repeat that the decrease in μ_y/μ_x below the m_x/m_y value means that the anisotropy in the scattering times increases. Only for $\mu_y/\mu_x=m_x/m_y$ the scattering time is isotropic $\tau_x=\tau_y$.

Interestingly, we empirically find that results of μ_y/μ_x for different w collapse onto a single curve provided the density axis is scaled properly with a scaling factor S_w. This scaling is shown in Fig. 4 for a set of QW widths and IS with impurities at the edge of the QW. We note that the scaling is exact at low densities and large well width, where $q \ll q_S$ and $k_x^F, k_y^F \gg 1/w$. In this case the scattering function depends only on the form factors F_C and F_I, which are functions of the product qw. Hence, as $k_x^F, k_y^F \propto N_S^{1/2}$, a scaling law with $S_w \propto w^2$ is expected. In our case the scaling factor S_w is nearly proportional to $w^{3/2}$ as shown in the inset of Fig. 4. This behavior is intermediate between the quadratic behavior at low N_S and large w and the opposite case of high N_S and small $w \to 0$, where the scaling factor is width independent.

The mobility μ_x and the mobility ratio μ_y/μ_x for IRS versus N_S are shown in Fig. 5. μ_x decreases with increasing N_S, reaches a minimum at $N_S \approx N_S^* \equiv g_v/(2\pi\Lambda^2)$ and increases again (not shown) owing to a reduction in the random potential by the factor $\exp(-k_x^{F^2}\Lambda^2)$. Similar results have been found for the isotropic QW.[11] Note that the mobility ratio is strongly enhanced $\mu_y/\mu_x \approx 12 > m_x/m_y$=5.5 for $N_S < 2 \times 10^{11}$ cm^{-2}. This enhancement has its origin in the q dependence of the scattering probability, which increases with wave number as $Q(q \to 0) \propto q^2$ in the case of IRS. This increase is a screening effect. At higher density, where the screened random potential is strongly reduced by the exponential factor, the ratio μ_y/μ_x decreases. Still, even for high $N_S \approx 10^{12}$ cm^{-2} the mobility ratio remains larger than the mass ratio, see Fig. 5(b). Note, see Fig. 5(a), that the mobility $\mu_y \propto \mu_x \propto w^6$ increases strongly with increasing w so that IRS in (110) AlAs QWs is only relevant in high mobility samples (with low N_I) with small well width. The IRS might become more relevant in future, when cleaner samples are

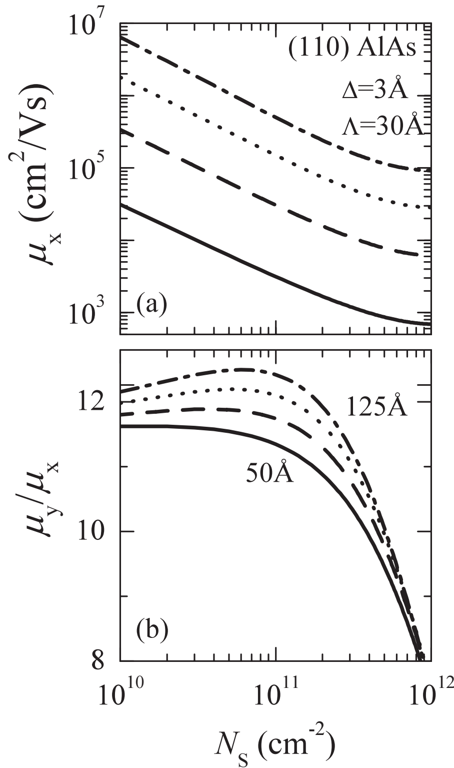

FIG. 5. (a) Mobility μ_x and (b) mobility ratio μ_y/μ_x versus electron density N_S for (110) AlAs QWs for IRS for different well width $w=50$ Å (solid line), $w=75$ Å (dashed line), $w=100$ Å (dotted line), and $w=125$ Å (dashed-dotted line).

available and the numbers for N_I become smaller.

Comparing Fig. 3 with Fig. 5 we conclude that mobility ratios can give information about the disorder present in a sample. The analysis of experimental results is easy if only one scattering mechanism is present. Of course, in a real sample always both scattering mechanisms, IS and IRS, are present and the interpretation is more involved.

As an example for a crossover behavior between IS and IRS we show in Fig. 6 the mobility and the mobility ratio versus N_S if both scattering mechanisms are present. While at low carrier density IS is dominant, see the dashed thin line in Fig. 6(b) and at high-density IRS is dominant, see the other dashed thin line. Between 10^{11} cm^{-2}$<N_S<$$10^{12}$ cm^{-2} a crossover from IS to IRS occurs. Of course, if experiments are made in this crossover regime the interpretations of experimental results is only possible when a detailed comparison with theory is made. For μ_y/μ_x the crossover occurs at relatively large N_S and therefore the large $\mu_y/\mu_x \approx 12$, expected for IRS in the low N_S range, is not observed in Fig. 6. For future samples with much lower impurity density this would change dramatically, as the crossover regime shifts to lower density.

Finally, we stress that the results shown in this paper for (110) AlAs should qualitatively apply to (110) AlP QWs. We mention that the isotropic electron gas on the (100) AlP surface has been studied recently.[21] The effective-mass ratio in (110) AlP system is $m_x/m_y \approx 3$. Our calculations should also be of relevance for (110) $Si_{1-x}Ge_x$ QWs. Very high mobility values for (100) Si QWs have been reported recently.[22] Detailed calculations will be made when experimental results on the band structure (valley degeneracy) and transport data are available for the anisotropic case (110).

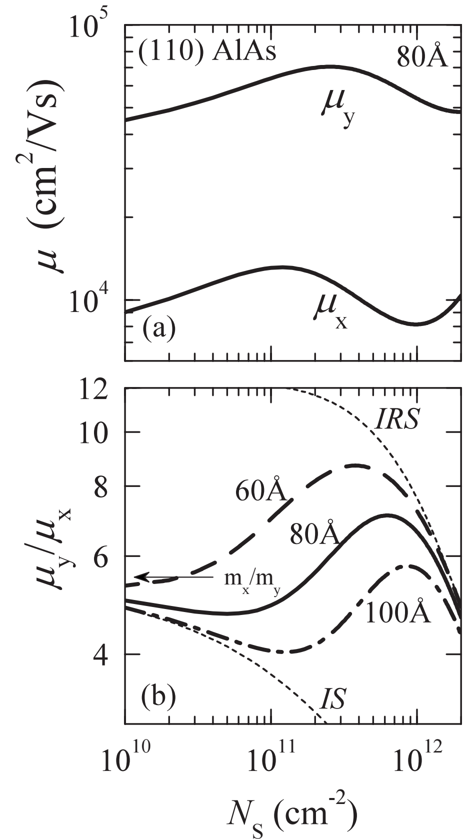

FIG. 6. (110) AlAs quantum well with IS ($N_I=1\times10^{10}$ cm^{-2} and $z_I=0$) and IRS ($\Delta=3$ Å and $\Lambda=30$ Å). (a) Mobility μ_x and μ_y versus electron density N_S for $w=80$ Å. (b) Mobility ratio μ_y/μ_x versus N_S for different well width $w=60$ Å (dashed line), $w=80$ Å (solid line), and $w=100$ Å (dashed-dotted line). The dashed thin lines describe a single-scattering mechanism (IS or IRS) for $w=80$ Å. The arrow represents the mass ratio.

V. (110) SILICON MOSFET STRUCTURES

Experimental values for the mobility in Si(110) MOSFET structures are in the range of $\mu_x \approx 10^3$ cm^2/V s.[2] This forces us to use a high density of impurities $N_I=1\times10^{12}$ cm^{-2} in the calculations. We assume that the impurities are located at the Si/SiO_2 interface, i.e., $z_I=0$. Note that in typical high mobility samples of (100) MOSFET structures the impurity density is much lower: $N_I \approx 1\times10^{11}$ cm^{-2}. It is not clear why the number of impurities in (110) Si MOSFET structures is so high.[2,17–20] For the IRS parameters we use the same values as for AlAs: $\Delta=3$ Å and $\Lambda=30$ Å.

The mobility μ_x and the mobility ratio μ_y/μ_x for IS and impurities at the interface versus N_S are shown in Fig. 7 for two values of the valley degeneracy. Thanks to screening effects the mobility for $g_v=4$ is, at low N_S, a factor 4 larger than for $g_v=2$. With increasing density the mobility increases, due to screening. The ratio μ_y/μ_x decreases with increasing density due to screening and the form factors F_I

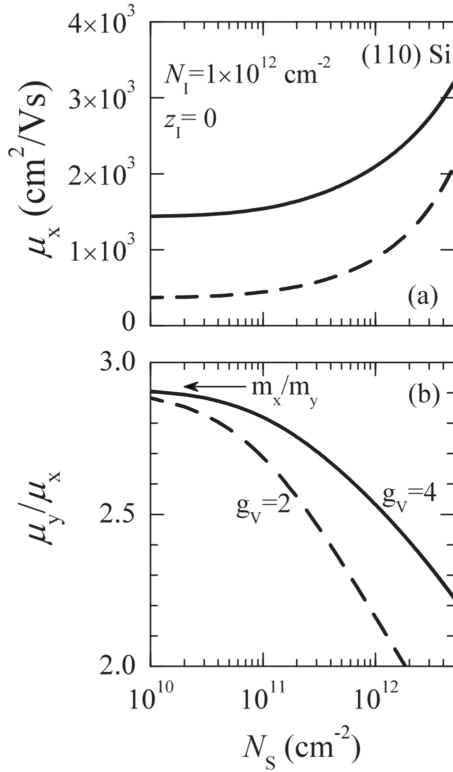

FIG. 7. (a) Mobility μ_x and (b) mobility ratio μ_y/μ_x versus electron density N_S for (110) Si MOSFET structures for IS with impurities located at the interface $z_I=0$ and for valley degeneracy $g_v=2$ (dashed line) and $g_v=4$ (solid line). The arrow represents the mass ratio.

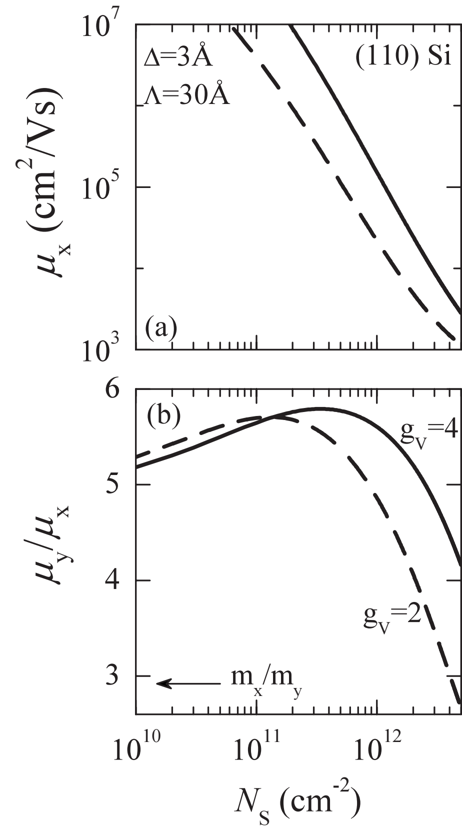

FIG. 8. (a) Mobility μ_x and (b) mobility ratio μ_y/μ_x versus electron density N_S for (110) Si MOSFET structure for IRS for valley degeneracy $g_v=2$ (dashed line) and $g_v=4$ (solid line). The arrow represents the mass ratio.

and F_C, as typical for IS. We repeat that this decrease in μ_y/μ_x means that the anisotropy in the scattering times increases and for IS one has again $\tau_x>\tau_y$. For finite density, say $N_S=3\times10^{11}$ cm^{-2}, there exists a significant difference of μ_y/μ_x for $g_v=2$ and 4. We suggest that this could be used to get more information about the valley degeneracy in (110) MOSFET structures.

The mobility μ_x and the mobility ratio μ_y/μ_x for IRS versus density N_S are shown in Fig. 8 for different valley degeneracy. μ_x strongly decreases with increasing N_S because the electron gas is pushed toward the interface so that $Q(q)\propto N_S^2$. Similar results have been found for isotropic (100) MOSFET structures.[7] Note that the mobility ratio is strongly enhanced compared to the mass ratio, $\mu_y/\mu_x\approx5.5>m_x/m_y=2.9$, nearly by a factor 2 for not too high N_S. This enhancement is quite similar to what was found for AlAs QWs. At higher density the ratio μ_y/μ_x decreases because of $Q(q)\propto\exp(-k_F^2\Lambda^2)$.

The crossover behavior between IS and IRS is shown in Fig. 9, where the mobility and the mobility ratio versus density are shown when both scattering mechanisms are present. A characteristic peak mobility is found, similar to (100) Si MOSFET structures.[7] For $N_S<10^{12}$ cm^{-2} the mobility ratio is dominated by IS, see the dashed thin line in Fig. 9(b). Only for high N_S IRS becomes important.

An experimental result for $N_S=3.15\times10^{12}$ cm^{-2} from Ref. 2 is shown as a solid dot with $\mu_y/\mu_x=1.83$.[23] The comparison between theory and experiment for μ_y/μ_x shown in Fig. 9(b) is encouraging. We do not perform the best fit to this single experimental point because the number of parameters in the theory is too big to make such a fit reliable. Instead, we demonstrate that the theory has enough freedom to improve the agreement with experiment. It has been shown for QWs that placing the impurities away from the center of the electron gas, for instance at the edge, can considerably reduce the mobility ratio.[6]

In Fig. 10 we have shown for IS the ratio μ_y/μ_x versus impurity position z_I for impurities located in the SiO_2. The electron density used $N_S=3.15\times10^{12}$ cm^{-2} corresponds to the experimental value of Ref. 2. With increasing z_I the ratio μ_y/μ_x is substantially reduced and can reach values as low as $\mu_y/\mu_x\approx1.2$, much lower than the experimental value $\mu_y/\mu_x\approx1.83$.[2] Hence, the experimental value seen in Ref. 2 might be explained by impurities located in the oxide. We hope that more systematic studies are performed for (110) Si MOSFET structures in order to test our predictions.

Our results for (110) Si MOSFET structures should also be applicable to $Si_{1-x}Ge_x$ heterostructures,[24,25] where z_I is the spacer distance for remote doping. The only difference between MOSFET structures and heterostructures is the dielectric constant, which is higher in the latter case $\varepsilon_L\approx12.5$. Numerically, we find that the mobility ratio is not very sensitive to the dielectric constant. Therefore experiments with (110) Si heterostructures could test the predictions of Fig. 10, at least qualitatively.

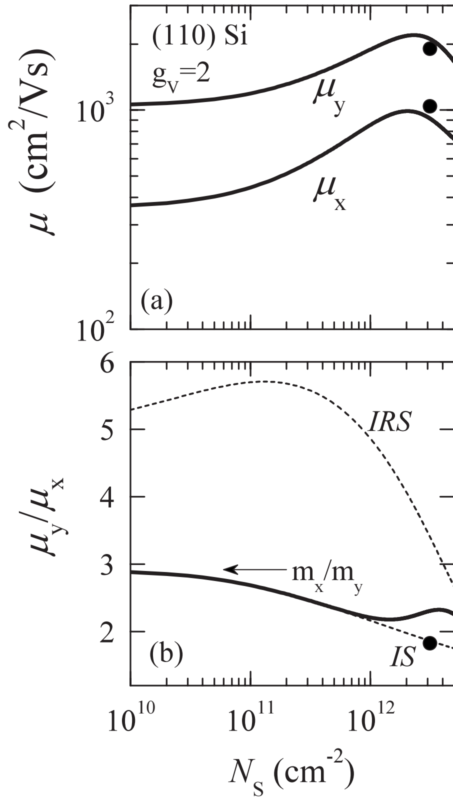

FIG. 9. (110) Si MOSFET structures with IS (N_I=1 $\times 10^{12}$ cm^{-2} and z_I=0) and IRS (Δ=3 Å and Λ=30 Å) for g_v =2. (a) Mobility μ_x and μ_y versus electron density N_S. The solid dots are experimental results of Ref. 2. (b) Mobility ratio μ_y/μ_x versus N_S for IS and IRS as the solid line. The dashed thin lines represent a single-scattering mechanism (IS or IRS). The solid dot represents the experimental result of Ref. 2. The arrow represents the mass ratio.

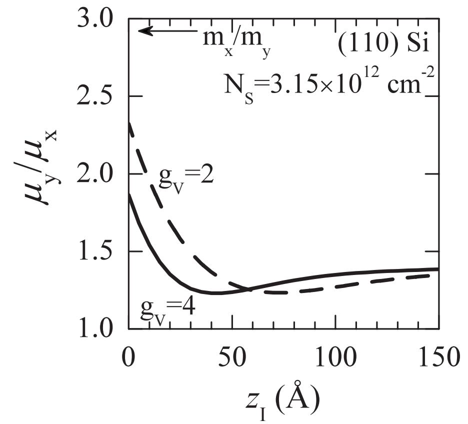

FIG. 10. Mobility ratio μ_y/μ_x for (110) Si MOSFET structures versus impurity position z_I for impurities located in SiO_2 for different valley degeneracy. The electron density is N_S=3.15 $\times 10^{12}$ cm^{-2}, as in the experiment of Ref. 2. The arrow represents the mass ratio.

VI. DISCUSSION

From our numerical results we conclude that the mobility ratio is sensitive to the origin of disorder. We conclude that if $\mu_y/\mu_x > m_x/m_y$ the dominant scattering mechanism is IRS. For $\mu_y/\mu_x < m_x/m_y$ the dominant scattering is expected to be IS, if the density is not too high. Impurity scattering is sensitive to the position of impurities, as one can see in Fig. 10 for MOSFET structures (for QWs see Ref. 6). We propose that measurements of the mobility anisotropy can be used to get insight into the disorder present in real samples. This is very interesting for samples growers. We hope that our work initiates a more systematic experimental research on the anisotropic mobility in two-dimensional systems, especially because comparison with theoretical predictions now is possible.

In the following we discuss assumptions and approximations used. The calculations are done in lowest order of the disorder and multiple-scattering effects are neglected. In general one can say that multiple-scattering effects become important for low mobility.[26] Because of the high mobility in the (110) AlAs QW used in Ref. 3 we expect that multiple-scattering effects are not important for that sample. However, such effects can already be important for the (110) Si MOSFET structure studied in Ref. 2. We hope that systematic studies of samples with lower mobility (higher disorder) and near the metal-insulator transition could give valuable information about multiple-scattering effects. In addition many-body effects due to exchange and correlations, which can be described by a local-field correction,[27] have been neglected in our calculations because expressions for anisotropic systems are not available in the literature. Many-body effects are expected to be more important for low electron density. It is not excluded that for the mobility ratio these corrections partly cancel out. Only systematic studies of the anisotropic mobility versus density of high mobility samples can help to get experimental information about this effect.

We stress that in the present paper we have studied only isotropic scattering potentials. The anisotropy comes in from the anisotropic effective mass via the Vogt-Herring-type transformation and the fact that we take into account the electron-electron interaction, which makes the screened random potential strongly q dependent. In calculations, where the Coulomb interaction effects are neglected, one needs to introduce unphysical anisotropic scattering potentials in order to explain $\mu_y/\mu_x \neq m_x/m_y$.[28] In comparing experimental results[2,3] with theory we have supposed that anisotropic scattering potentials are not present. It is, however, known that anisotropic scattering potentials exist, for instance in GaAs, for a discussion see Ref. 5. Such potentials also contribute to anisotropic transport.

Concerning real samples we stress that the impurity distribution in samples used in experiments often is not really known. Systematic measurements and comparison with theory is needed and will help to get more information on the position of impurities. We hope that our calculations motivate experimenters to do such experiments. Finally, we mention that transport measurement of the isotropic two-dimensional electron gas have been used for decades in order to get information about disorder and/or new ground states. The field of transport properties of the anisotropic two-dimensional electron gas is (i) completely open from an experimental point of view and (ii) provides additional predic-

tive power from a theoretical point of view, due to the *two* mobilities μ_x and μ_y.

Another topic could be an effective mass depending on the electron density, as found in (100) Si MOSFET structures.[29] It could be interesting to see whether a similar effect exists in an anisotropic electron gas.

VII. CONCLUSIONS

We calculated the anisotropic conductivity in (110) AlAs quantum wells and (110) Si MOSFET structures at zero temperature and to the lowest order in the disorder. Detailed predictions have been made for impurity scattering, interface-roughness scattering, and for both scattering mechanisms coexisting. Strong anisotropic mobilities and anisotropic scattering times are found. For a mass ratio $m_x/m_y=2.9$ in (110) Si MOSFET structures we find mobility anisotropies in the range $1.2<\mu_y/\mu_x<6$, corresponding to $1/2<\tau_y/\tau_x<2$. Our predictions can be tested in experiment. Measurements of the anisotropic conductivity can be used to get information about the disorder and the Coulomb interaction in real samples. The calculations also apply qualitatively to (110) AlP quantum wells, (110) $Si_{1-x}Ge_x$ quantum wells, and (110) $Si_{1-x}Ge_x$ heterostructures.

---

*Permanent address: Institute of Solid State Physics, 142432 Chernogolovka, Moscow District, Russia.

[1] C. Herring and E. Vogt, Phys. Rev. **101**, 944 (1956).
[2] D. Bishop, R. C. Dynes, B. J. Lin, and D. C. Tsui, Phys. Rev. B **30**, 3539 (1984).
[3] S. Dasgupta, S. Birner, C. Knaak, M. Bichler, A. Fontcuberta i Moral, G. Abstreiter, and M. Grayson, Appl. Phys. Lett. **93**, 132102 (2008).
[4] H. Sakaki and T. Sugano, Jpn. J. Appl. Phys. **10**, 1016 (1971).
[5] Y. Tokura, Phys. Rev. B **58**, 7151 (1998).
[6] V. T. Khrapai and A. Gold, Pis'ma Zh. Eksp. Teor. Fiz. **90**, 389 (2009) [JETP Lett. **90**, 346 (2009)].
[7] T. Ando, A. B. Fowler, and F. Stern, Rev. Mod. Phys. **54**, 437 (1982).
[8] T. J. Drummond and I. J. Fritz, Appl. Phys. Lett. **47**, 284 (1985).
[9] M. Shayegan, E. P. De Poortere, O. Gunawan, Y. P. Shkolnikov, E. Tutuc, and K. Vakili, Phys. Status Solidi B **243**, 3629 (2006).
[10] A. Gold and R. Marty, J. Appl. Phys. **102**, 083705 (2007).
[11] A. Gold, Phys. Rev. B **35**, 723 (1987).
[12] A. Gold, Solid State Commun. **60**, 531 (1986).
[13] R. E. Prange and T. W. Nee, Phys. Rev. **168**, 779 (1968).
[14] V. S. Khrapai, JETP Lett. **77**, 317 (2003).
[15] J. M. Ziman, *Principles of the Theory of Solids* (Cambridge University Press, Cambridge, 1972).
[16] S. Dasgupta, C. Knaak, J. Moser, M. Bichler, S. F. Roth, A. Fontcuberta i Moral, G. Abstreiter, and M. Grayson, Appl. Phys. Lett. **91**, 142120 (2007).
[17] A. A. Lakhani and P. J. Stiles, Phys. Lett. A **51**, 117 (1975).
[18] T. Neugebauer, K. von Klitzing, G. Landwehr, and G. Dorda, Solid State Commun. **17**, 295 (1975).
[19] K. C. Woo and P. J. Stiles, Surf. Sci. **113**, 278 (1982).
[20] T. Cole and B. D. McCombe, Phys. Rev. B **29**, 3180 (1984).
[21] M. P. Semtsiv, S. Dressler, W. T. Masselink, V. V. Rylkov, J. Galibert, M. Goiran, and J. Leotin, Phys. Rev. B **74**, 041303 (2006).
[22] T. M. Lu, D. C. Tsui, C.-H. Lee, and C. W. Liu, Appl. Phys. Lett. **94**, 182102 (2009).
[23] The electron density $N_S=3.15\times10^{12}$ cm^{-2} used in Ref. 2 was very special: $\mu_x=1041$ cm^2/V s, $\mu_y=1903$ cm^2/V s and $\rho_{xx}=1/\sigma_{xx}=1903\ \Omega$, $\rho_{yy}=1/\sigma_{yy}=1041\ \Omega$.
[24] F. Schäffler, Semicond. Sci. Technol. **12**, 1515 (1997).
[25] T. M. Lu, J. Liu, J. Kim, K. Lai, D. C. Tsui, and Y. H. Xie, Appl. Phys. Lett. **90**, 182114 (2007).
[26] A. Gold and W. Götze, Phys. Rev. B **33**, 2495 (1986).
[27] D. Pines and P. Noziéres, *The Theory of Quantum Liquids* (Benjamin, New York, 1966).
[28] P. Wölfle and R. N. Bhatt, Phys. Rev. B **30**, 3542 (1984).
[29] S. V. Kravchenko and M. P. Sarachik, Rep. Prog. Phys. **67**, 1 (2004).